Fachtagung "Lasermethoden in der Strömungsmesstechnik"
9. – 11. September 2014, Karlsruhe

Untersuchungen an einer abgelösten Triebwerksgondel bei gestörter Zuströmung

Investigations in a Stalling Nacelle Inlet with Disturbed Onstream

Simon Übelacker, Rainer Hain, Christian J. Kähler

Institute of Fluid Mechanics and Aerodynamics, Universität der Bundeswehr München,
Werner-Heisenberg-Weg 39, 85577 Neubiberg

Durchflussgondel, PIV, Wirbelgenerator
Flow-through nacelle, PIV, vortex generator

Summary

A flow-through nacelle was investigated at the Institute of Fluid Mechanics and Aerodynamics at the Universität der Bundeswehr in Munich. The boundary layer loading of the nacelle resembles that of a powered engine at take-off conditions and high mass flow rates. The aim of the project is to generate an experimental validation database in order to develop a physically based numerical code to calculate the flow at the edge of the flight envelope. The investigations concentrated on the flow under an inhomogeneous onstream. Therefore, a vortex generator was positioned 1.74 m in front of the nacelle's leading edge. This vortex generator is a motor driven airfoil, which pitches from angles of attack of α_{vg} = -11° to α_{vg} = 11° within approximately 60 ms.

Introduction

In a time of increasing air traffic, reliable numerical codes for the calculation of wing and nacelle stall are required. Moreover, the expansion of the flight envelope's edge has recently been a challenging task for the industry and the engineering sciences. The Deutsche Forschungsgemeinschaft Research Group 1066 "Simulation of Wing and Nacelle Stall" is developing different numerical codes for the flight at the edge of the aircraft's envelope. A general overview about this work is given in Radespiel et al. 2013 and Niehuis et al. 2013.

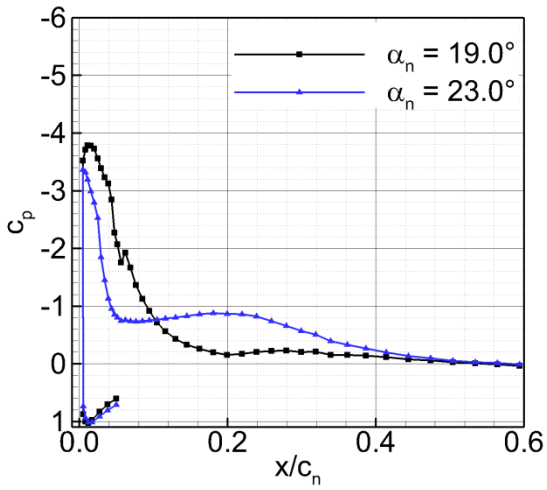

Fig. 1: Pressure distribution in the inlet

Validation experiments are required for the development of numerical models. Therefore, a cold flow-through nacelle was investigated at the Institute of Fluid Mechanics and Aerodynamics at the Universität der Bundeswehr München. Recent investigations focused on the start and landing period of the aircraft (i.e. low speed and high

angles of attack). During this phase of flight a turbulent separation bubble can develop in the front part of the intake. Figure 1 shows the pressure distribution in the inlet of the examined model. The pressure coefficient c_p is plotted against the x-coordinate in the main flow direction starting at the leading edge of the model. The static pressure is measured in the inner mid section of the nacelle between 0 and 60% of the chord. While at $\alpha_n = 19°$ the boundary layer is still attached, at $\alpha_n = 23°$ a turbulent separation has formed. The separated region is characterized by the plateau of the pressure.
Nacelle stall is a highly unsteady phenomenon. Vortices develop and are shed downstream. Therefore, an interaction with the compressor is likely. A vortex can hit the blade and locally change the angle of attack of the blade. This can cause stall to the compressor. Stall or rotating stall leads to total pressure losses in the compressor. The total pressure loss decreases the efficiency of the compression stage of the engine. Additionally, atmospheric turbulence is relevant when the airplane is flying close to the ground. Gusts can hit the inlet and interact or even cause the separation. The aim of this work was to investigate the interaction of a generic vortex with the flow and the separation in the inlet.

Experimental setup

A cold flow-through nacelle was used for the investigations, see Fig. 2 (a). The axially symmetric model has a chord length of $c_n = 526$ mm and a leading edge diameter of 315.6 mm. The nacelle was developed on the basis of the Laminar Flow Research Action (LARA) nacelle, see Schulze et al. 2007. As the experiments were performed at a relatively low onflow Mach number $Ma = 0.11$, the separation is not shock induced as in the LARA nacelle. Therefore, the shape of the inner side of the nacelle was modified in order to achieve a pressure induced separation, see Schulze 2013. The front part of the model is made from Plexiglas® to allow for optical access, whereas the rear part, which connects the model with the sting, is made from steel. All presented experiments were performed at a Reynolds number of $Re_{cn} \approx 1.25 \cdot 10^6$. The Reynolds number is based on the chord length of the nacelle. The experiments were conducted at the atmospheric wind tunnel Munich. This facility is an Eiffel-type wind tunnel with a closed test section. The dimensions of the test section are 1.85 m × 1.85 m × 20 m. The maximum velocity of this facility is $U_\infty = 40$ m/s. Conventional static pressure measurements were performed in order to find the angle of attack with separation onset. It became apparent that separation occurs at $\alpha_n \approx 21°$.
The investigations focused on the interaction between the inlet stall and the inhomogeneous

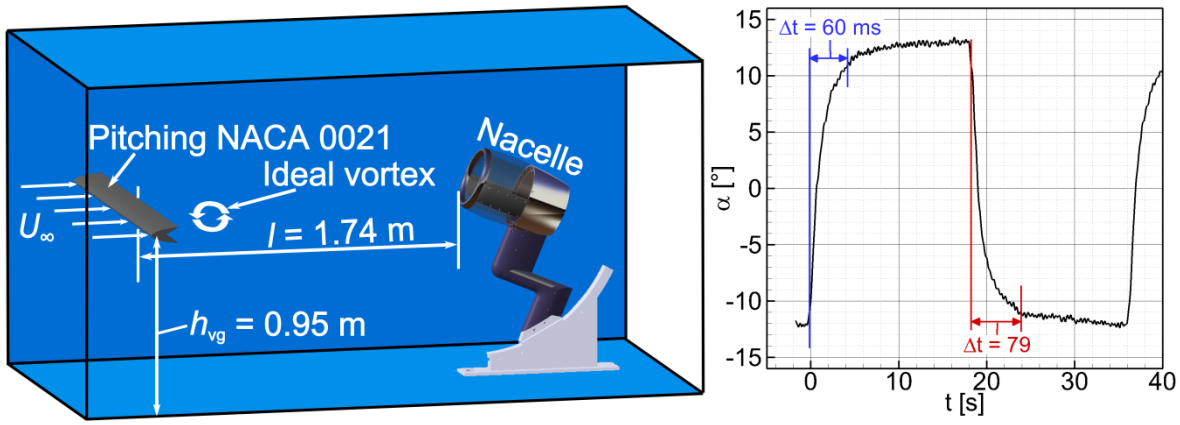

(a) Experimental Setup (b) Pitch of the vortex generator

Fig. 2: Experimental setup with the vortex generator 1.74 m upstream of the nacelle (left). Potentiometer data of the pitching airfoil (right)

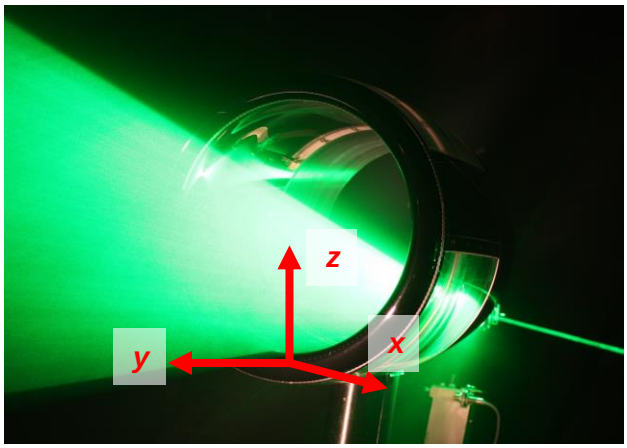

Fig. 3: Light sheet

onstream. Flow distortions can occur while the airplane is flying through gusty conditions. The distortions can be critical at the edge of the flight envelope. In order to generate a gust in the wind tunnel, a distortion generator was developed, see Hahn et al. 2012. This vortex generator is a pitching airfoil, which was positioned 1.74 m upstream of the nacelle, see Fig. 2 (a). Two linear motors on each side are moving the airfoil from outside the wind tunnel. The airfoil is a NACA 0021 with a chord length of c_{vg} = 160 mm. The airfoil's shell is made from carbon fiber laminate. The vortex generator moves from α_{vg} = -11° to α_{vg} = 11° within 60 ms, pauses at approximately α_{vg} = 11° for 195 ms, moves back to α_{vg} = -11° within 79 ms, and pauses at α_{vg} = -11° for approximately 168 ms. In Fig. 2 (b) the angle of attack of the vortex generator is plotted against the time. These data are acquired with a potentiometer. The plot shows that one cycle lasts 500 ms. By moving from α_{vg} = -11° to α_{vg} = 11°, lift increases due to the change of the circulation around the airfoil and therefore a starting vortex develops. This starting vortex is a counter clockwise rotating vortex. In this investigation, the interaction of the turbulent separation bubble with the counter clockwise rotating vortex was of main interest. This vortex is considered critical due to the fact that it primarily increases the angle of attack of the nacelle before the angle of attack is reduced.

In order to achieve an interaction of the convecting vortex and the turbulent separation bubble, the airfoil of the vortex generator was mounted at a height of 950 mm from the ground of the wind tunnel. In the investigated range of the nacelle's angle of attack (between α_n = 19° and α_n = 23°), the leading edge of the nacelle has also a height of approximately 950 mm from the ground, see Fig. 2 (a). Due to the curvature of the streamlines because of the lift of the nacelle the vortex is convected through the nacelle.

The presented measurement techniques are static pressure measurements, see Fig. 1, and Stereoscopic Particle Image Velocimetry (SPIV). Besides, time resolved pressure measurements in the inlet were performed in order to acquire the fluctuations of the static pressure as well as to detect the interaction between the vortex and the nacelle. Furthermore, threads were attached in the region of the turbulent separation bubble to determine the symmetry of the flow in the intake. The results of the latter method indicate that in the majority of the cases the flow can be considered symmetrical.

For the mentioned SPIV experiments two high-speed CMOS Cameras (Imager pro HS 4M) were installed above the test section at a distance of approximately 1.3 m from the field of view. The spatial resolution is reduced to 2016 px × 704 px. At this resolution a maximum, frame rate in the double frame mode of this camera is 1800 Hz. In this mode, the camera acquires single images with twice the frequency (i.e. 3600 Hz). The maximum frequency was exploited in these measurements only to acquire a single cycle of the vortex generator (500 ms) in order to achieve the maximum time resolution. However, the SPIV results presented in this paper correspond to data acquired at a frame rate of 1000 Hz in the double frame mode. The presented measurements were conducted in the symmetry plane of the nacelle, see Fig. 3. Moreover, the measurements at steady state of the vortex generator were acquired at 100 Hz in the double frame mode in order to obtain uncorrelated vector fields. The laser light sheet was inserted into the axially symmetric nacelle from downstream, see Fig. 3. The light sheet thickness was 2 mm to 3 mm. A Zeiss Makro Planar T*2/100 lens

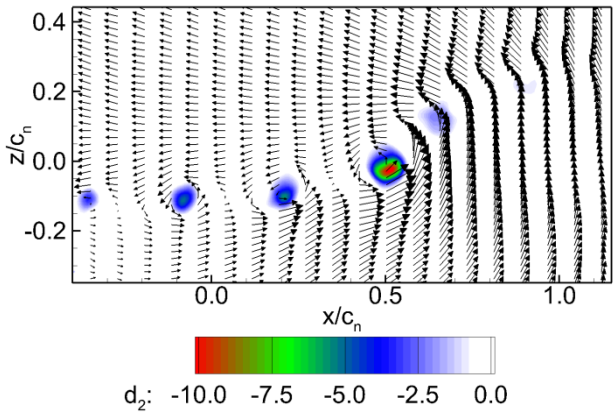

Fig. 4: Wake of the vortex generator

was used. The SPIV validations were carried out with a decreasing window size from 64 px to 32 px and 50% interrogation window overlap.
The trigger signal was set when the vortex generator was passing $\alpha_{vg} = -10°$. The measurement was started with a short delay of 12 ms to 33 ms and 30 images to 105 images were acquired. This cycle was repeated 1000 times. Therefore, 1000 vector fields were averaged for consecutive times after the trigger signal. The time delay and the number of acquired images were chosen to guarantee sufficient time to record the vortex convecting through the nacelle. The presented results are for $\alpha_n = 19°$ and for $\alpha_n = 23°$. Therefore, the attached case as well as the separated angle of attack will be discussed, see Fig. 1.

Results

Due to the change in angle of attack of the symmetric airfoil of the vortex generator, a vortex develops and is convected downstream. Former planar PIV measurements indicate that several single vortices (visualized by the d_2-criterion) develop, see Fig. 4. This criterion separates vortices from other patterns, see Vollmers 2001, and is given by

$$d_2 = (\partial u/\partial x + \partial w/\partial z)^2 - 4\cdot\left(\partial u/\partial x \cdot \partial w/\partial z - \partial u/\partial z \cdot \partial w/\partial x\right). \quad (1)$$

While u is the velocity component in the x-direction, w is the velocity in the z-direction. Figure 4 shows the wake of the vortex generator at the position of the nacelle but without the nacelle in the wind tunnel. The origin of the Cartesian coordinate system is the bottom leading edge of the nacelle, see Fig. 3. In Fig. 4, the freestream velocity was subtracted from the vector field. The colored area shows the relevant values of the d_2-criterion. It becomes apparent that, due to some instability the vortex decays in several single vortices. Without the nacelle in the test section no significant shift of the height of the convecting vortices is observed.
In Figs. 5 and 6 the averaged absolute flow field is shown. The black contour is the nacelle's bottom leading edge. Figures (a) display the result for the time t = 35 ms after the trigger signal of the vortex generator, whereas Figs. (b) illustrate the vector field for the time t = 56 ms after the trigger signal. The time was counted from the airfoil passing $\alpha_{vg} = -10°$, see Fig. 2 (b). In Fig. 5 the angle of attack of the nacelle is $\alpha_n = 19°$ and in Fig. 6 the angle of attack is $\alpha_n = 23°$. The absolute velocity in the plane of the main flow direction is given as

$$|U_{xz}|/U_\infty = \sqrt{(u/U_\infty)^2 + (w/U_\infty)^2}. \quad (2)$$

The velocity vectors are averaged over 1000 vector fields.
In Fig. 5, it becomes apparent that the absolute velocity at the leading edge is higher compared to $\alpha_n = 23°$ in Fig. 6. This results in a higher suction peak and is shown in Fig. 1. Figure 6 (b), when t = 56 ms, also shows that the separation is slightly bigger compared to t = 35 ms. This is indicated with the bigger blue area, which shows an area of low absolute velocities. At an angle of attack of $\alpha_n = 19°$ the velocities are decelerated as well at t = 56 ms. This is indicated by a bright green area downstream of the leading edge in the near-wall region in Fig. 5 (b). To conclude, the distortions by the vortex lead to changes in the onstream to the compressor and can therefore change the mechanical loads on the compressor.

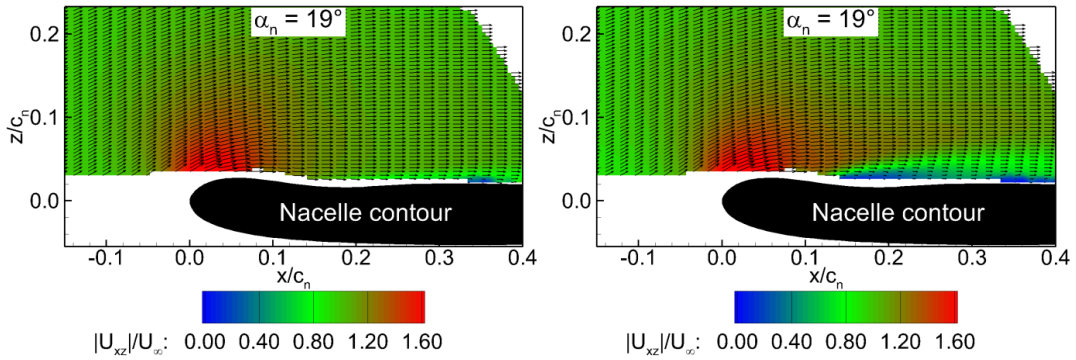

(a) t = 35 ms (b) t = 56 ms

Fig. 5: Mean in-plane flow field at α_n = 19°

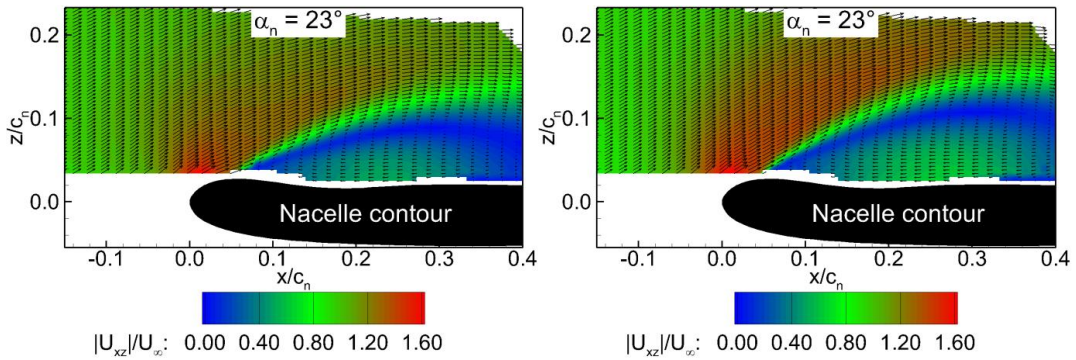

(a) t = 35 ms (b) t = 56 ms

Fig. 6: Mean in-plane flow field at α_n = 23°

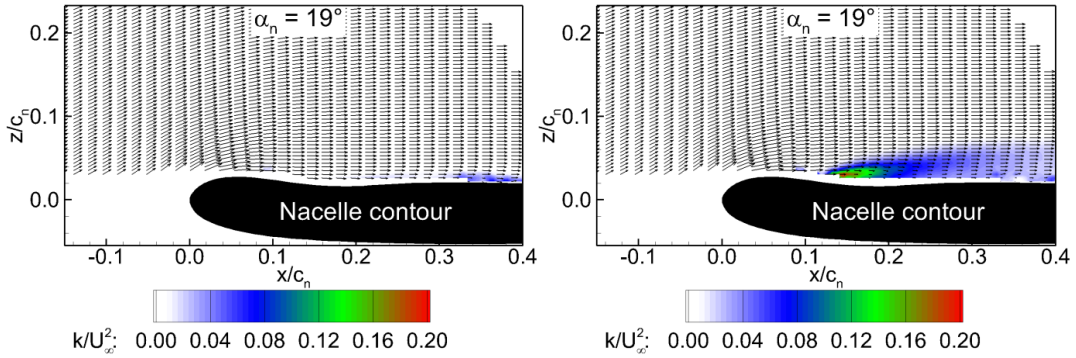

(a) t = 35 ms (b) t = 56 ms

Fig. 7: Normalized turbulent kinetic energy at α_n = 19°

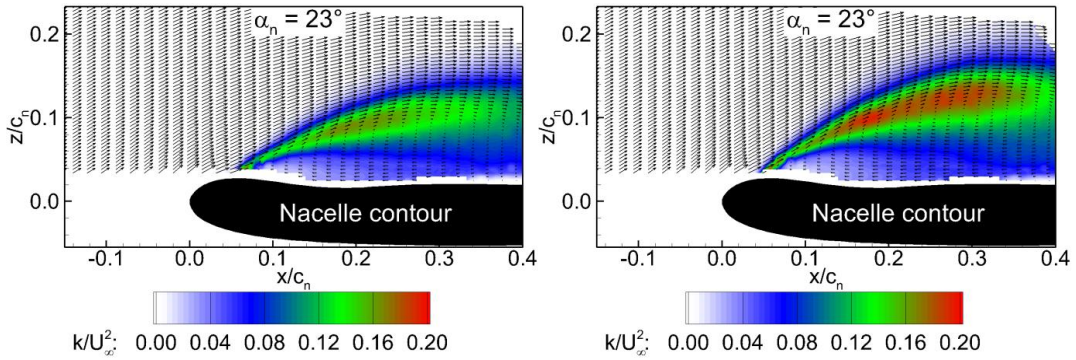

(a) t = 35 ms (b) t = 56 ms

Fig. 8: Normalized turbulent kinetic energy at α_n = 23°

Figures 7 and 8 show the normalized turbulent kinetic energy for the same angles of attack and the corresponding times of Figs. 5 and 6. The arrangement of the Figs. 7 and 8 is consistent with the Figures above. It can be clearly seen that the level of turbulent kinetic energy is relatively high at α_n = 23° compared to α_n = 19°. This is a result of the separated flow at the higher angle of attack. At the time t = 56 ms it is also apparent that the fluctuations of the three velocity components are higher than at t = 35 ms. This result indicates that the counter clockwise rotating vortex enlarges the fluctuations in the flow. If the separation is already present, the separated region will also be increased. Therefore, the impact of the distortion on the flow through the nacelle is considered to be significant and to destabilize the flow in the intake of the engine.

Fig. 2 (a) shows that the vortex generator's trailing edge was placed 1.74 m upstream of the nacelle's leading edge. The convection time of the vortex between the vortex generator and the nacelle is expected to be approximately 47 ms since the experiments are carried out at onstream velocities between U_∞=35.5 m/s and 39 m/s. Therefore, the expected value is slightly smaller than t = 56 ms. This is due to the fact that the time is counted from the initial movement of the vortex generator, while passing α_{vg} = -10°.

In Fig. 9 an equidistant time series of vector fields of the interaction between the vortex and the nacelle is shown at α_n = 19°. The black contour is the bottom leading edge of the nacelle, whereas the white point indicates the position, where the Probability Density Function (PDF) of the normalized stream-wise velocity fluctuations u' are calculated, see Fig. 10. The histograms were calculated using 1000 single vector fields at a certain time t. The colors in Fig. 9 indicate the absolute normalized in-plane velocity fluctuations given as

$$\left(\left|\dot{U}_{xz}\right|/U_\infty\right)_{\alpha_{vg}=-11°} = \sqrt{\left(\dot{u}_{\alpha_{vg}=-11°}/U_\infty\right)^2 + \left(\dot{w}_{\alpha_{vg}=-11°}/U_\infty\right)^2}. \qquad (3)$$

While u' is the velocity fluctuation in the x-direction, w' is the velocity fluctuation in the z-direction. The index α_{vg} = -11° indicates that the mean vector field with the vortex generator at a steady angle of attack of -11° was subtracted from the correspondent phase averaged velocity field at time t. Both mean vector fields were averaged over 1000 single vector fields.

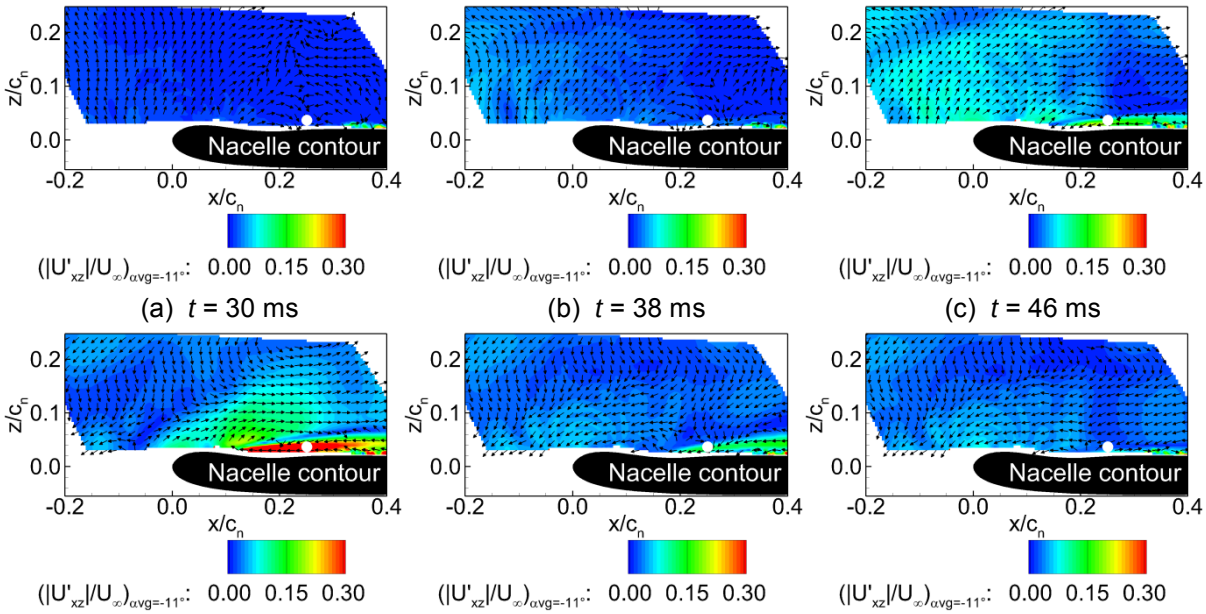

Fig. 9: Absolute in-plane fluctuation velocities at α_n = 19°

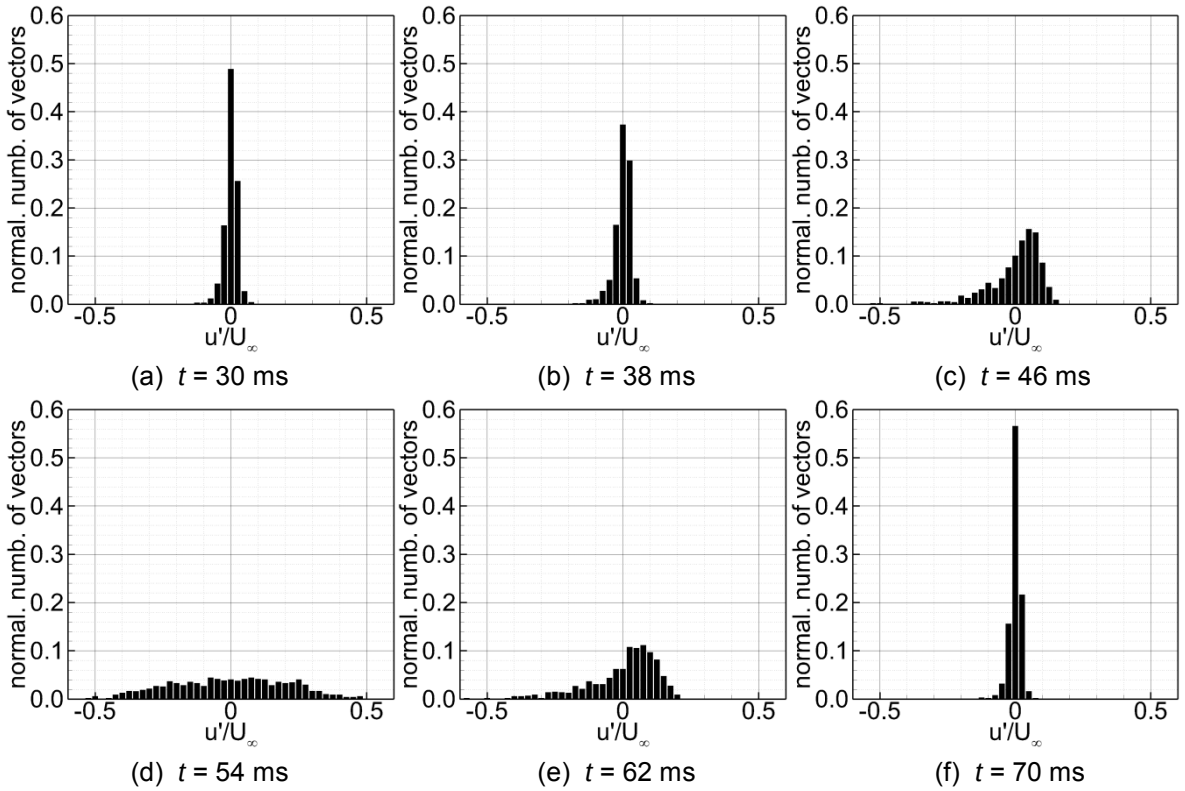

Fig. 10: Histograms of the normalized velocity fluctuation u'/U_∞ for different times t at $\alpha_n = 19°$

The vectors in Fig. 9 show the fluctuation velocities $u'_{\alpha vg = -11°}$ and $w'_{\alpha vg = -11°}$. While Fig. 9 shows the periodic distortion, Fig. 10 shows the turbulent distortion by the vortex. The time spacing between the plotted vector fields is 8 ms. The influence of the counter clockwise rotating vortex on the flow field can be clearly seen in Figs. 9 (c) – 9 (e). The near-wall distortions are particularly high in Fig. 9 (d). Therefore, the PDF of the fluctuation velocities u' were calculated in this area. Note that the histograms were calculated for the phase averaged fluctuation velocities. The number of vectors was normalized with the total number of vector fields (i.e. 1000). The bin-width was chosen as $u/U_\infty = 0.025$. Figure 10 shows that the fluctuation velocities are relatively small at t = 30 ms, t = 38 ms and t = 70 ms, whereas the fluctuations during the distortion at t = 46 ms to 62 ms are a lot higher. At time t = 54 ms the fluctuation velocities reach an absolute value of $u'/U_\infty = 0.8$ even at the attached angle of attack of the nacelle (i.e. $\alpha_n = 19°$). These fluctuations are convected downstream and can cause problems at the fan (e.g. stall, rotating stall, or blade vibrations). The histograms in Figs. 10 (c) and 10 (e) show that the fluctuation velocities can also have an unbalanced distribution.

The effect of the vortex generator on the separated flow has already been shown in Figs. 6 and 8. However, the effect of the vortex on the probability for reversed flow in the nacelle will be discussed below. Figure 11 shows the ratio of the number of reversed vectors to the total number of vectors downstream the leading edge of the nacelle R_{rev} plotted against the time. This ratio is given by

$$R_{rev} = \left.\frac{\text{Number of vectors}|_{u/U_\infty < 0}}{\text{Total number of vectors}}\right|_{x/c_n \geq 0}. \quad (4)$$

It becomes apparent that the peak in both curves is at $t \approx 58$ ms. This value is higher than the expected convection velocity of the vortex due to the fact that the time is counted from the initial movement of the vortex generator and the vortex needs some time to develop. Figure 11 also shows that the initial state of the ratio of reversed vectors to the total number of

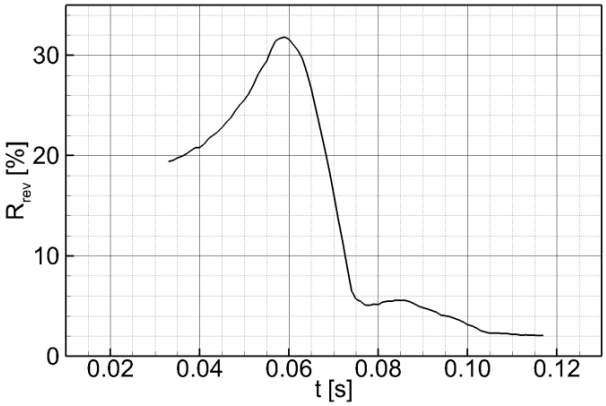

Fig. 11: Probability for reversed flow at $\alpha_n = 23°$

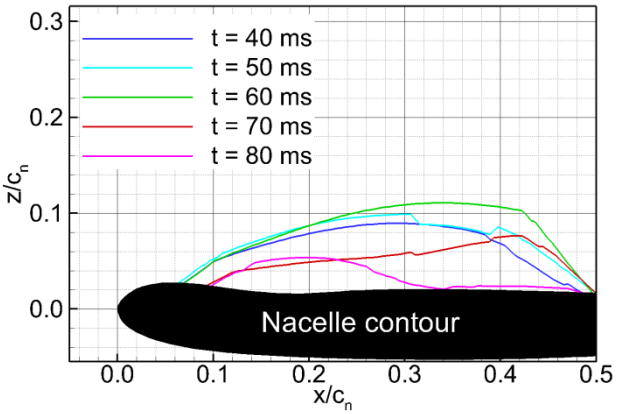

Fig. 12: Lines of $u'/U_\infty = 0$ at $\alpha_n = 23°$

vectors downstream the nacelle's leading edge is not equal to the final state. The reason for that is that the induced velocity due to the vortex generator's airfoil at steady state according to the Biot-Savart law. While at $\alpha_{vg} = -11°$ the effective angle of attack of the nacelle is increased, the effective α_n is reduced at $\alpha_{vg} = 11°$. This phenomenon leads to a shift of separation onset. Therefore at $\alpha_{vg} = 11°$, separation onset is shifted towards higher angels of attack. The shift of separation onset was shown in static pressure measurements. At $\alpha_n = 23°$, when a relatively big turbulent separation bubble has already formed, this effect leads to a decrease of the ratio of reversed flow R_{rev}, see Fig. 11.

Figure 12 shows the contour lines of the velocity $u/U_\infty = 0$ for different times t in the inlet. This zero velocity in the x-direction indicates the dynamics during the impingement of the vortex on the nacelle. The lines were derived from the SPIV results at each vector position. At $t = 40$ ms (blue line) the contour of zero velocity has a certain size, which increases up to $t = 60$ ms. The maximum extension in the radial direction is almost 10% of the nacelles chord, while the axial size of the contour line is approximately 50% of the chord at $\alpha_n = 23°$. The amount of reversed velocities decreases after $t \approx 58$ ms, as shown in Fig. 11. This also means that the contour line of zero velocities $u/U_\infty = 0$ decreases, see Fig. 12. It is also shown that the initial state is not the final state, due to the induced flow field by the vortex generator. Additionally, a deformation of the red line ($t = 70$ ms) of zero velocity can be discovered in Fig. 12.

Conclusion

The motivation of this experimental investigation was to examine the effect of an atmospheric distortion on the attached as well as the separated flow in a nacelle. The experimental results are a unique validation database in order to develop sophisticated numerical models to calculate the flow at the edge of the flight envelope. The measurements were performed at high angles of attack and low Reynolds numbers of $Re_{cn} = 1.25 \cdot 10^6$. The investigated model is a generic axially symmetric flow-through nacelle. The boundary layer loading of the nacelle is similar to that of a powered jet intake during take-off and landing and high mass flow rates, see Schulze 2013. Distortions are generated by a pitching airfoil in the test section upstream of the nacelle in order to simulate an atmospheric gust. These distortions are judged to have a critical effect on the inlet separation, as the turbulent separation bubble is increased in size by the interaction with the counter clockwise rotating vortex, see Fig. 6. This result was expected as the rotation of the vortex initially increases the angle of attack of the nacelle. The onflow upstream to the compressor is changed significantly. This can change the mechanical loads on the compressor or lead to total pressure losses and therefore reducing the efficiency of the engine. The ratio of reversed vectors to all vectors downstream the leading edge of

the nacelle, indicates that the region of reversed flow is primarily increased. The velocity induced by the vortex generator's airfoil leads to a difference between the initial and the final state of the ratio of the number of reversed vectors to the total number of vectors, see Figs. 11 and 12. Investigations of experiments with attached flow in the nacelle at α_n = 19° indicate that the generated distortion has a crucial effect as well. The periodic distortions as well as the turbulent fluctuations in the near-wall region are increased while the vortex interacts with the nacelle, see Figs. 9 and 10.
It can be concluded that the vortex generator is adequately constructed to disturb the flow field in this model significantly. The vortex is convected with the free stream velocity of the wind tunnel. The validation of the unsteady pressure measurements, as well as the time resolved SPIV validation, will show if the vortex shedding is influenced by the distortion as well. Furthermore, the effect of the clockwise rotating vortex on the flow has to be investigated.

Acknowledgments

The authors would like to thank the Deutsche Forschungsgemeinschaft for funding the research within the framework of the research group 1066 "Simulation of wing and nacelle stall".

References

Hahn, D., Scholz, P., Radespiel, R., 2012: "Vortex Generation in a low speed wind tunnel and vortex interactions with a high-lift airfoil", 30th AIAA Applied Aerodynamics Conference, doi: 10.2514/6.2012-3024, New Orleans, Louisiana

Niehuis, R., Lesser, A., Probst, A., Radespiel, R., Schulze, S., Kähler, C.J., Spiering, F., Kroll, N., Wartzek, F., Schiffer, H.-P., 2013: "Simulation of Nacelle Stall and Engine Response", Proceedings of the XXI. International Symposium on Air Breathing Engines (ISABE), Busan, Korea

Radespiel, R., Gisele Francois, D., Hoppermann, D., Klein, S., Scholz, P., Wawrzinek, K., Lutz, T., Auerswald, T., Bange, J., Knigge, C., Raasch, S., Kelleners, P., Heinrich, R., Reuß, S., Probst, A., Knopp, T., 2013: „Simulation of Wing Stall", 43rd AIAA Fluid Dynamics Conference, doi: 10.2514/6.2013-3175, San Diego, California

Schulze, S., Kähler, C.J., Radespiel, R., 2007: "On the Comparison of Stalling Flow-Through Nacelles and Powered Inlets at Take-Off Conditions", 1st CEAS European Air and Space Conference, Berlin, Germany

Schulze, S., 2013: „Experimentelle Untersuchungen zur Wirbeldynamik am überziehenden Triebwerkseinlauf", Shaker Verlag, Aachen, Germany

Vollmers, H., 2001: "Detection of vortices and quantitative evaluation of their main parameters from experimental velocity data", Meas Sci Technol, 12, pp. 1199-1207